



Flexural Behavior of Hybrid Fiber Reinforced SCC Beams with Longitudinal and Bubble Voids

Esraa M. Edaan ^{1*}, Shatha D. Mohammed ¹

¹ Department of Civil Engineering, College of Engineering, University of Baghdad, Baghdad 17001, Iraq.

Received 09 January 2025; Revised 01 March 2025; Accepted 11 March 2025; Published 01 April 2025

Abstract

To investigate the flexural behavior of self-consolidating hybrid fiber-reinforced concrete beams containing voids experimentally, six RC beams were tested, one solid without fiber and the others containing hooked-steel and macro-polypropylene fibers with a volume fraction of 1 and 0.5%, respectively. One of the five fibrous beams was solid; two contain a series of recycled plastic balls of diameters 110 and 120 mm, and another two contain a single longitudinal circular void created by PVC pipes of diameters 90 and 110 mm. The flexural behavior of the beams was assessed depending on the load-deflection curve, load-strain curve, ductility, toughness, stiffness, and crack patterns. The experimental outcomes showed that all the tested specimens (solid and voided) failed in a flexural mode. Hybrid fiber inclusion in the solid beam improved the load capacity at different loading levels, enhanced the stiffness by 38.3%, and increased the absorbed energy by 29.55%. The presence of voids in fibrous beams decreased the loads at cracking, yielding, and ultimate stages and enhanced the ductility. The ductility index, depending on deflection and energy methods, showed higher values for voided beams. The toughness of voided beams at the ultimate stage was enhanced by 1.1% to 28%. The voided beams exhibited lower values of stiffness, and their values decreased when the diameter of the voids increased. The outcomes also indicated that the incorporation of hybrid fiber significantly minimized the strain in steel reinforcing bars at the post-cracking stage, and the presence of voids minimized the reduction effect of steel strain according to void size and shape.

Keywords: Hybrid Fiber; Steel Fiber; Polypropylene Fiber; Voided Beam; Flexural; Self- Compacted Concrete.

1. Introduction

The incorporation of voids and longitudinal holes within beams leads to a decrease in their own weights. As a result, the necessary dimensions of supporting structural elements like foundations and columns are reduced, which would lead to less material consumption for construction. Additionally, the presence of these holes offers the opportunity to accommodate crucial utility services, including sewage systems, ducts for air conditioning, water supply, and electrical and telephone wiring, via the beams, wherever necessary [1, 2]. The application of void formers in concrete has several benefits, including:

- Flexibility in design that allows for easier adaptation to curved and irregular layouts, larger spans, and less supports [3].
- Cost reduction: reduced material consumption and accelerated construction processes [3].
- Reduction in dead weight by approximately 37 %, leading to reduced foundation sizes.
- Column spacing was increased by up to 50% compared to traditional constructions.

* Corresponding author: e.edaan1901p@coeng.uobaghdad.edu.iq

<http://dx.doi.org/10.28991/CEJ-2025-011-04-08>



© 2025 by the authors. Licensee C.E.J, Tehran, Iran. This article is an open access article distributed under the terms and conditions of the Creative Commons Attribution (CC-BY) license (<http://creativecommons.org/licenses/by/4.0/>).

- Reduced foundation dimensions, allowing for a decrease of up to 50% in structural dead load.
- Reduced concrete consumption, with one kilogram of recycled plastic replacing one hundred kg of concrete.
- Eco-friendly and sustainable approaches that reduce energy consumption and carbon footprint. Cement production accounts for 8% of global CO₂ emissions [4].
- Enhanced beam's dynamic response since it caused a reduction in the inertia force [5].
- Utilization of recycled materials.

The transformation from compression to the tension region of the conventional beam when the load is applied creates an ineffective area at the central section of the neutral axis because this section experiences lower tension and compression than the regions above and below the neutral axis [6]. In recent years, many researchers have concentrated on the effect of longitudinal holes on the load capacity, ductility, and stiffness of RC beams. Studies related to this topic may be categorized according to their type (experimental, analytical, and numerical), hole size (big and small), and hole shape (circular, rectangular, and square). Many investigations were made on the voided beams with rectangular and square longitudinal holes. Abbass et al. [7] examined the flexural performance of voided high-strength concrete beams; findings indicated that the beam featuring a square hole with a volume reduction of 16 % and 28 % exhibited greater ductility than the solid beams, while the hollow beam with a concrete volume decrease of 44 % demonstrated ductility like the solid beam. Nuaimi et al. [8] studied the performance of solid beams experimentally and compared it with the square voided RC beams under combined loadings. The results indicated the solid specimen fractured and failed at greater loads than the voided one. Additional studies were found that examined the structural performance of circular hollow RC beams. The size and position of the circular opening have a significant impact on the strength and stiffness of the voided beam [9]. The structural performance of circular hollow RC beams with a circular shape is better than square and rectangular ones because stress is concentrated near sharp edges. Murugesan & Narayanan [10] examined the flexural behavior of R.C. hollow beams with simple supports. Thirteen RC beams of dimensions 1700×150×150 mm were statically tested. One of these beams was solid, and another twelve beams had longitudinal circular holes of diameter 25, 40, and 50 mm, and the location of the center of the hole also changed from 45 to 180mm. Theoretical equations were developed to estimate the load capacity of RC voided beams. The results indicated that the increasing hole size resulted in a decrease in load value at both the first crack and ultimate phases. It is also demonstrated that the load-bearing capacity of voided RC beams containing a longitudinal opening completely located in the stress block was lower than that of all other beams. The ultimate load was greater than that of the other hollow beams when the longitudinal hole was completely under the stress block.

The behavior of circular hollow reinforced SCC beams was experimentally studied by Ismael & Hameed [11]. Optimization analysis was also carried out to identify the optimal hollow section. Additionally, a sustainability evaluation was conducted on the hollow beam type to evaluate its efficacy in reducing CO₂ emissions, usage of natural resources, and embodied energy. Six beams measuring 150, 100, and 1000 mm were exposed to a gradually applied load until they failed. Five specimens featuring longitudinal circular voids of diameters 32, 36, 40, 46, and 52 mm in compression to the control solid beam, the outcomes indicated that it could decrease the concrete used in SCC beams by 5.4 to 14.2%, alongside a decline in the cracking load by 9.1 to 22.7% and the load capacity by 2.3 to 10.5%, respectively. Among all these beams, the optimization analysis showed that the hollow-core beam with a diameter of 46 mm was the optimal option for minimizing concrete volume by 11.1 %, in addition to a 13.6% decrease in cracking load and a 9.3% reduction in ultimate load. The use of longitudinal voids of diameters ranging from 32 to 52 mm is recommended by the sustainability analysis, which led to reduced carbon dioxide emission by 5.4 to 14.1%. The ductility of hollow-core reinforced concrete beams was enhanced by enlarging the diameter of the longitudinal void. Al-Smadi et al. [12] made experimental and analytical studies on the effects of longitudinal holes with different shapes, sizes, and positions on the structural behavior of RC beams. Nine specimens of dimensions 150×250×1300 mm with three void types, the first created by PVC pipes with two sizes, 50 and 75 mm; the second created by a rectangular MDF wooden tube (50×100 mm); and the last provided by a square (50×50 mm) MDF tube. Each hole was fixed at two positions (90 & 160 mm) from the upper surface of the specimen. All specimens failed in a flexural tensile mode inside of varying hole shapes and sizes. The load capacity in hollow beams was lower by a maximum reduction of 20 % than the solid beam, according to the opening size and shape.

Sivaneshan & Harishankar [13] studied experimentally the behavior of six reinforced voided concrete beams. One solid and others voided with polyethylene balls of 75, 65, and 35 mm diameter. The results indicate that the ultimate load and first crack load for voided beams were less than solid beams. Ajeel et al. [14] conducted experimental tests on a voided RC beam, two solid beams, two containing recycled plastic spheres, and one involving a pipe. Two beams (solid and containing plastic spheres) were tested under a pure moment, and the others were tested under combined moments. The outcomes revealed that under the bending moment, the ultimate strength was less than the solid one by 13-23% and also less in stiffness and the first crack load by 10 %, while for a combined moment, the reduction was about 35 % in the first crack load and 30 % in the ultimate load.

The effectiveness of various reinforcement materials on the structural response of multi-hollow RC beams featuring longitudinal voids with thin walls separating them was explored by Hekal et al. [15]. In this study, sixteen beams with different reinforcement materials, involving steel bars, glass fiber polymer, geogrid mesh, basalt fiber polymer, expanded steel mesh, and carbon fiber strips, were tested. The researchers aimed to find the best options for making strong, lightweight beams that can handle heavy loads without cracking. The outcomes indicated that multi-hollow RC beams with steel bars produced 75% capacity of solid RC beams with a weight reduction of 40%, and with CFRP produced 83.3% capacity of solid RC beams with 40% weight reduction.

From the research outcomes mentioned above, it was noticed that the sectional area reduction of the beam led to reducing its strength and large deformation, to overcome those problems, the concrete mix materials could be developed by including a certain quantity of fibers (steel or synthetic) into the concrete mix. Numerous researches on the structural behavior of fiber-reinforced concrete beams, more specifically, steel fiber-reinforced concrete beams, have been performed in the literature [16-19]. According to these investigations, fibers increase ultimate strength, fracture energy, and stiffness; decrease extensive crack width; lessen concrete beam deflection; and regulate crack propagation. The capacity of steel fibers in concrete to distribute tension strains throughout the fractured portion and provide residual strength is one of the fibers' most crucial roles. The distribution of the fiber and the interfacial contact between the fiber and the concrete matrix affect the amount of residual strength.

Hybrid fiber concrete may also be made by combining different fiber types in the matrix, such as using steel and polypropylene fibers to reinforce plain concrete [20]. Utilizing the unique qualities of each fiber while combining the mechanical features of two or more distinct fibers is the primary goal in the creation of hybrid fiber concrete. The self-compacted method allows for uniform distribution of fibers without the need for vibration, which can lead to better mechanical properties and enhance the workability and flowability. The inclusion of fibers in SCC mixtures improves the toughness, ductility, and flexural capacity of the concrete, as fibers help to bridge cracks and distribute loads more evenly [21]. It is necessary to combine fibers of high modulus and great flexibility with fibers of high modulus and poor flexibility, like merging a high tensile modulus fiber such as steel, carbon, and glass fiber with low modulus and high flexibility such as polypropylene and nylon fibers, where high modulus fiber provides high flexural strength and stiffness, but the low modulus fibers enhance the post-cracking behavior that improves the ductility and absorbed energy of the structural member [22]. The structural behavior of hybrid fiber RC beams has been widely studied, revealing significant enhancements in flexural performance due to various fiber types and dosages. Wu et al. [23] demonstrated that incorporating polyvinyl alcohol and polyethylene fibers notably increased stiffness and flexural capacity. An analytical model for bearing capacity and crack predictions was developed based on experimental data.

Yoo et al. [24] investigated the flexural behavior of reinforced ultra-high-performance fiber-reinforced concrete (R-UHPFRC) beams, particularly focusing on the effects of varying steel fiber volume fractions, aspect ratio, and type and their impact on mechanical properties. Eight RC beams of dimensions 150×185×1200 mm were tested, and three different steel fiber types were used. Short straight SS with volumetric ratio (0, 0.5, 1, 1.5, 2, 2.5, and 3), medium-length MS, and twist fiber TS with a ratio of 2%. It finds that adding steel fibers enhances tensile strength and energy absorption, with optimal performance at a volume fraction of 2.0%. However, the strain-hardening behavior of UHPFRC adversely affects cracking and stress redistribution, leading to reduced ductility indices. A fiber volume fraction of 1.0 or less resulted in strain-softening behavior. Sasikumar & Candassamy [25] reviewed the shear behavior of fiber-reinforced concrete (FRC) beams, emphasizing the significance of hybrid fibers in enhancing shear performance. By examining various combinations of metallic, synthetic, and biofibers, the research highlighted the synergistic effects of fiber volume, lengths, and orientations on improving the shear strength of reinforced concrete beams. The study underscored the importance of optimal fiber combinations and distribution to improve the overall shear resistance of FRC beams, offering valuable insights for future construction practices and materials engineering.

Alshahrani et al. [26] created advanced computer modeling to understand how steel fibers in self-compacting concrete can be arranged to improve its strength and performance after cracking. By exploring different ways to place these fibers based on the flow of SCC, random orientation, and longitudinal alignment, we can find the best method for creating strong and durable concrete structures. The concrete was modeled in a finite element program, Abaqus, by a damage plasticity model, and bond-slip behavior was implicitly included in the embedded fiber model formulation. The results showed that longitudinal fiber alignment significantly improves flexural strength by 104.4 % and toughness by 127.1%.

There are few studies on the use of fibers in voided beams. Altun et al. [27] investigated experimentally the flexural behavior of hollow beams with square holes. A steel fiber dosage of 30 kg/m³ was used for the SFRC beam. A central rectangular hollow part measuring 100 x 100 mm was present in three of the SFRC beams, whereas the last three featured a rectangular hollow part measuring 200 × 200 mm. The experimental outcomes indicated that the hollow SFRC box

beams exhibited a 29% lower ultimate load-carrying capacity than solid reinforced concrete beams, but their weight was 44% lighter, making them favorable for reducing external loads on structures like bridges. Jacob & Bincy [28] investigated the impact of steel fibers on the behavior of a hollow beam with a rectangular section and a circular longitudinal void. Through experimental work, eight RC beams of dimensions 150×150×1400 mm were tested, four without steel fiber and another four with steel fiber. PVC pipes of diameters 32, 40, and 50 mm were used to make longitudinal holes within the beams. The outcomes indicated that all tested beams with and without fiber failed in the flexural mechanism and hollow sections do not significantly decrease load capacity.

Additional research is required because the literature review does not provide a comprehensive assessment of the effects of hybrid fibers and the presence of voids with varying shapes on the flexural strength, ductility, stiffness, toughness, and crack propagation of RC beams. Therefore, the primary goal of this research is to better understand these issues by analyzing the overall behavior of hybrid fiber self-compacted reinforced concrete beams at different loading stages. This covers how hybrid fibers and voids affect the flexural members' deformability, ductility, stiffness, toughness, failure mode, and failure load. The present work investigates the structural behavior of hybrid fiber-reinforced self-compacted concrete beams with air voids. Six reinforced self-consolidating concrete beams were tested, one solid without fibers as a reference beam and the other five beams containing hooked-steel fiber and macro-polypropylene fiber with a volume fraction of 1% and 0.5%, respectively. One of the five fibrous beams was solid, two contained a series of recycled plastic balls of diameters 110 and 120 mm, resulting in a beam volume reduction of 8.13 and 9.81%, respectively, and another two contained a single PVC pipe of diameter 90 and 110 mm, resulting in a reduction in beam volume of 9.86% and 14.73%, respectively. The effects of hybrid fibers and voids on the flexural behavior of the RC beams were assessed depending on the load-deflection curve, load-strain curve, ductility, deformability, crack patterns, toughness, and stiffness. Figure 1 illustrates the methodology of the research followed in this study.

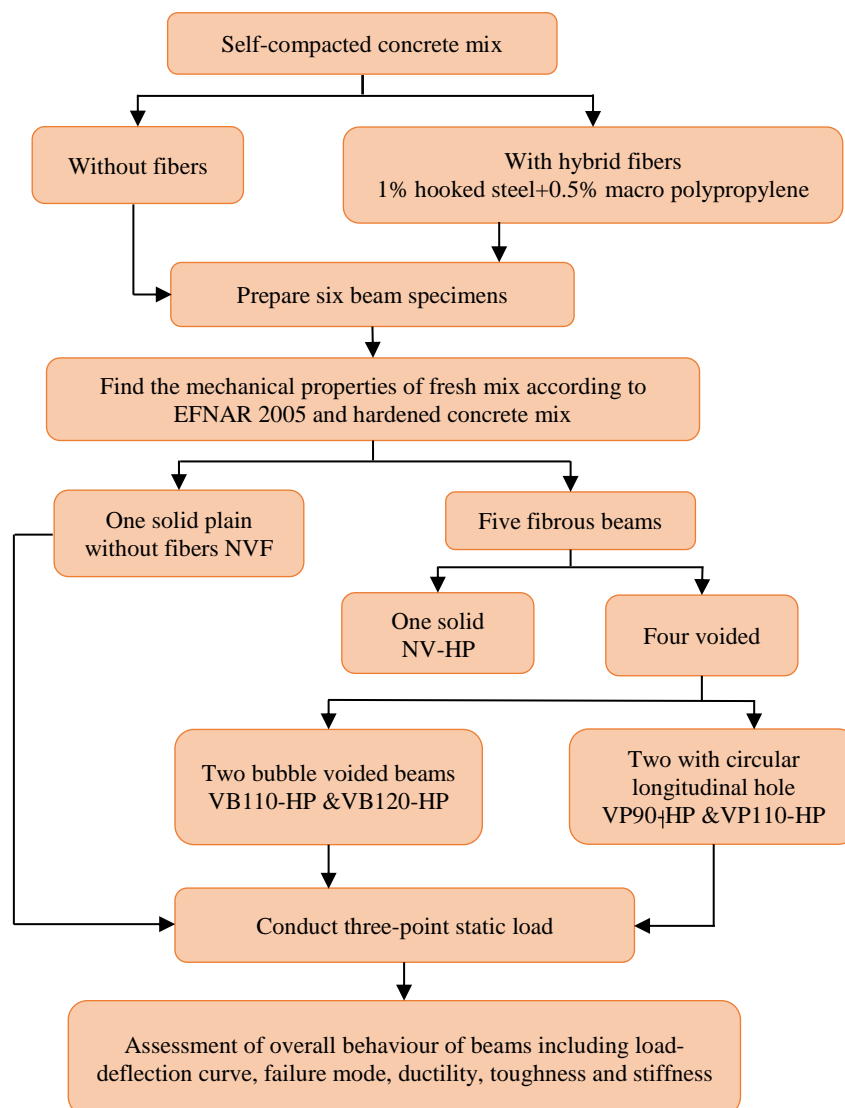


Figure 1. Methodology of the research

2. Experimental Work

2.1. Material and Mix Proportion

Beams in this study were cast using self-compacted concrete (SCC), which was designed according to the European Specification of Self-Compacted Concrete (EFNARC 2005) [29]. CEM I 42.5R Ordinary Portland Cement was used to prepare the concrete mixture. Crushed coarse aggregate with a maximum particle size of 10 mm and fine aggregate with a fineness modulus of 2.92 were employed. The grading analysis of both coarse and fine aggregate is shown in Figure 2 and validates the ASTM-C33/C33M-18 criteria [30].

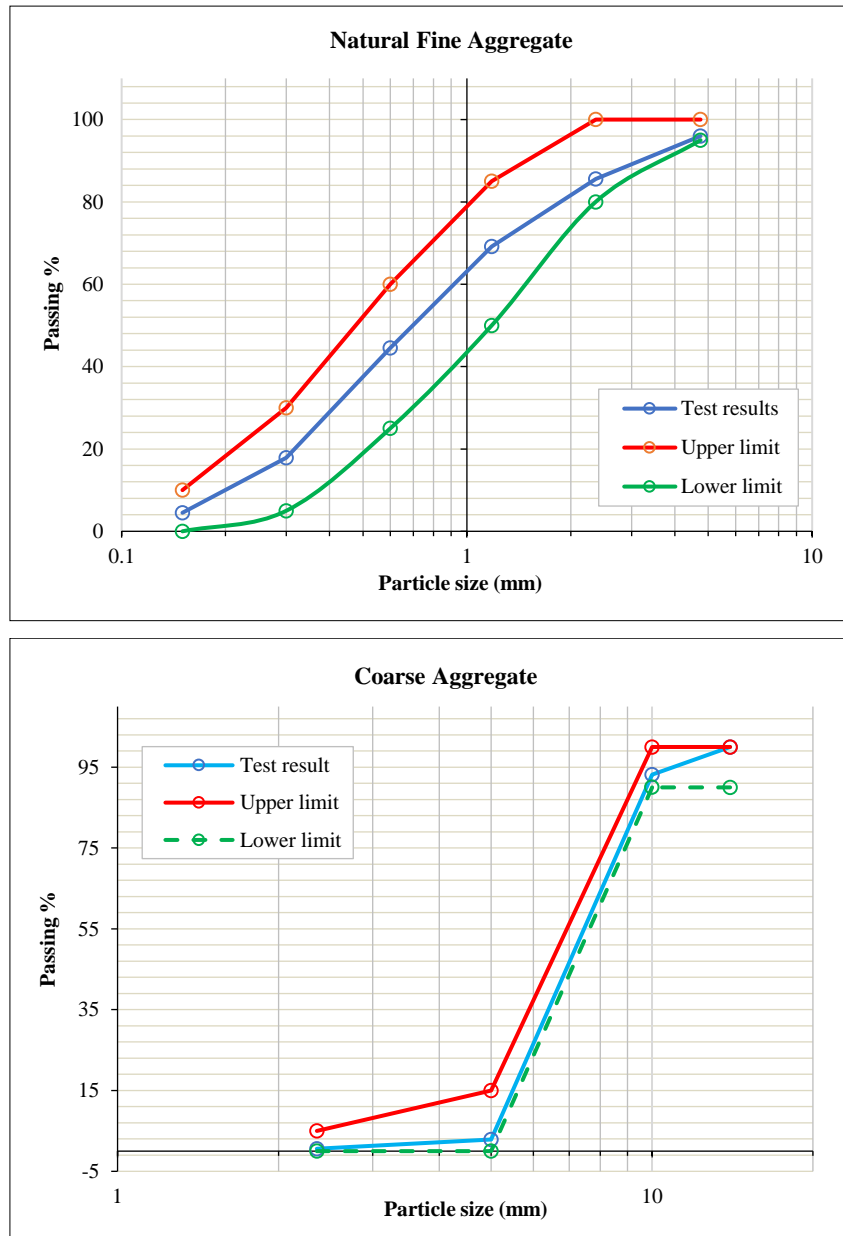


Figure 2. Grading analysis of fine and coarse aggregate

The silica fume utilized by the chemical business (COMIX), commercially called MegaAdd MS (D), was used as an additive (pozzolanic material) to produce the SCC for all specimens. A portion of the cement was replaced by 6% silica fume. Tap water was used for the concrete mix and curing. To enhance the workability of the concrete, a superplasticizer was incorporated into the mixture at a dosage rate of 2% by weight of the cement content. The mix proportions of materials per cubic meter (1 m³) of concrete are presented in Table 1. Hooked-end-type “TDS” steel fiber and “Sika forced-60” macro polypropylene (PP) fiber were used in the study. The steel fiber had a length of 35 mm and an aspect ratio of 64 with a diameter of 0.55 mm, while the PPF exhibited a length of 30 mm and an aspect ratio of 36 with a diameter of 0.84 mm. Hooked-steel fiber and macro-polypropylene fibers with a volume fraction of 1% and 0.5%, respectively, were used. The geometric and mechanical characteristics were obtained from the manufacturer and presented in Tables 2 and 3.

Table 1. Mix composition of concrete (kg/m3)

Cement	Sand	Gravel	water	SF*	SP*	Steel fiber	PPF fiber
490	798	810	183	30	9.8	78.5	4.55

* SF refers to amount of silica fume; SP refers to amount of superplasticizer

Table 2. Steel fiber properties

Configuration	Property	Specification
	Description	Hooked end
	Length	35 mm
	Diameter	0.55 mm
	Density	7800 kg/m ³
	Tensile strength	1000 -1100MPa
	Modulus of elasticity	200000 MPa
	Aspect ratio L/D,	64

Table 3. Properties of macro polypropylene fiber

Configuration	Property	Specification
	Description	deformed
	Length	30 mm
	Diameter	0.84 mm
	Density	910 kg/m ³
	Tensile strength	430 N/mm ²
	Modulus of elasticity	6 kN/mm ²
	Recommended dosage	3-10 kg/m ³

To confirm that the concrete mix utilized in this research was SCC, standard tests were performed to assess the properties of fresh self-compacting concrete (SCC) following EFNARC 2005 (slump flow and T50 test, the V-funnel test, and the L-Box-Test). The outcomes of these tests met the specifications outlined in EFNARC 2005, as demonstrated in Table 4 and Figure 3. The compressive strength of concrete was determined using cylindrical specimens with a diameter of 150 mm and a height of 300 mm. The testing procedures were conducted in accordance with the ASTM C39/C39M standard [31]. The average of the compressive strength of the three cylinders of each concrete mix type (plain and fibered concrete) at the test time was recorded as (f_c'). Also, three standard cubes of 150×150×150 mm for each plain and fiber concrete mix were used to estimate the cube's compressive strength (f_{cu}) for specimens at 28 days and at test time according to BS1811-116-11 (2011) [32]. The average of these three cube specimens was adopted as (f_{cu}). The splitting tensile strength of concrete (f_t) was determined based on ASTM C496/C496-M17 [33]. The modulus of elasticity of concrete (E_c) was determined in accordance with ASTM C469/C469-M14, utilizing standard 150 × 300 mm concrete cylinders [34].

Table 4. Properties of fresh self-compacted concrete mix

Test type	Parameters	Results	EFNARC (2005) Limits
Slump-Flow Test	Slump flow diameter (mm)	650	SF1 550-650
			SF2 660-750
			SF3 760-850
V-funnel Test	T ₅₀₀ (sec)	4.3	2-5
	T _V (sec)	8.76	6-12
	T _{5 min} (sec)	9.34	(6-12) +3
L-Box test	T _{20 cm} (sec)	1.45	-
	T _{40cm} (sec)	4.15	-
	BR%=H2/H1	0.91	0.8- 1



(a) slump flow and T_{50} test (b) the V-funnel test (c) L-Box test

Figure 3. Standard test for self-compacted concrete mix

To investigate the behavior of self-consolidating hybrid fiber RC beams containing air voids experimentally, six SCC beams were prepared. All the adopted specimens are identical in their dimensions (2400×300×200 mm). Flexural reinforcement included two tensile bars each measuring 12mm in diameter (a reinforcement ratio of 0.47 %). In addition, two compression top bars with a diameter of 6 mm. Transverse steel with a bar of 6 mm diameter was used as stirrups at a spacing of 100mm. The longitudinal and transverse reinforcement was designed following ACI-318-19 [35] to guarantee flexural failure and avoid any early shear failure. The reinforcement properties are summarized in Table 5, and the details of reinforcement and specimens are summarized in Table 6 and Figure 4. These beams were divided into five groups to study and analyze the following:

- The effect of hybrid fiber inclusion (1 % hooked end steel fiber & 0.5 % macro polypropylene fiber). This group involved two solid beams (NVF & NV-HP).
- The impact of bubble void diameter included two beams (VB110-HP & VB120-HP).
- The influence of longitudinal circular pipe diameter contained two beams (VP90-HP & VP110-HP).
- The effect of void shape resulted in the same concrete reduction volume of 9.8 %. This group consisted of two beams (VB120-HP & VP90-HP).
- The effect of void shape (bubble or pipe) with the same diameter included two beams (VB110-HP & VP110-HP).

Table 5. The mechanical characteristics of steel reinforcing bars

Nominal bar diameter (mm)	Measured diameter (mm)	Area (mm ²)	Weight (kg/m)	Yield strength (MPa)	Tensile strength (MPa)	Elongation %
6	6.06	28.93	0.2271	506.5	641.18	6%
12	11.73	108.06	0.8476	525.8	665.52	10%



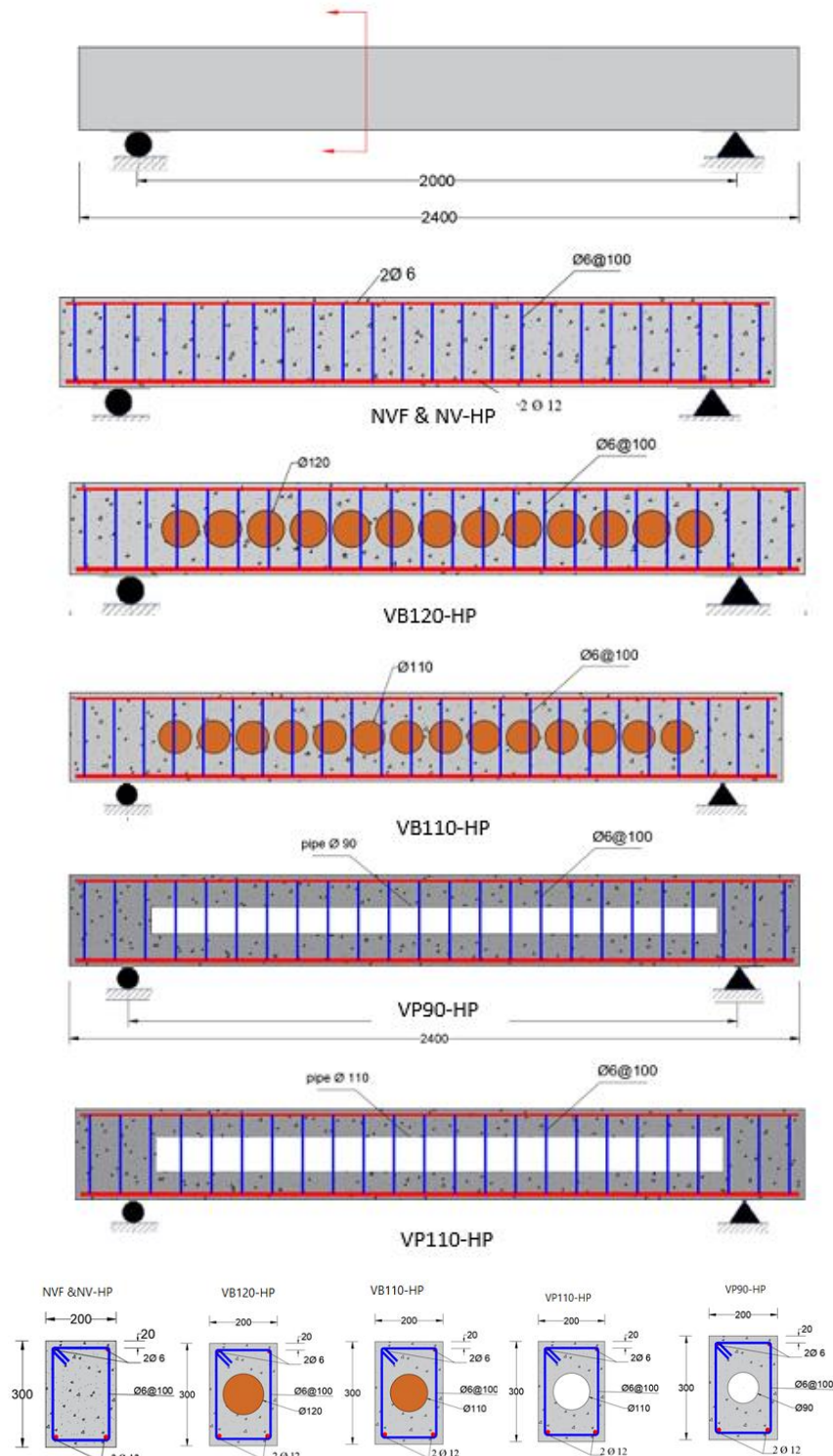


Figure 4. Beams preparation and details (all dimensions in mm unit)

Table 6. Details of Specimens

Beam Specimen	Volume Reduction %	Void type	Fiber's type & Volume fraction%	Steel fiber weight (kg/m ³)	PP fiber weight (kg/m ³)
NVF	-	-	-	-	-
NV-HP	-	-	-	-	-
VB120-HP	9.81	120 mm ball	Hooked steel (1.0) & Polypropylene (0.5)	78.5	4.55
VP90-HP	9.86	90 mm PVC pipe			
VB110-HP	8.13	110 mm ball			
VP110-HP	14.73	110 mm PVC pipe			

All specimens were tested under simply supported conditions, with an effective span of 2000 mm and a 200 mm extension at each end for the support system. Each specimen was loaded at mid-span by a gradual incremental monotonic concentrated load until failure occurred (when the load abruptly decreased as a result of either compressive concrete crushing or longitudinal rebar rupture, which are the two main flexural failure mechanisms). The load was applied gradually at a rate around 3 kN using a hydraulic jack with a maximum capacity of 500 kN. The applied load on the specimen was monitored using a load cell with a capacity of 1000 kN. Two LVDTs were employed to determine the vertical deflection of the beam. LVDT1 was positioned at the mid-span to capture the maximum deflection, while a second LVDT was placed near the support to monitor the rotation angle of the beam. A dial gauge was used to calibrate the readings of LVDT 1 (at mid-span). Strain gauges were used to measure the strains in the longitudinal steel reinforcing bars, stirrups, and concrete at several predetermined locations, as shown in Figure 5. The data acquisition system read and recorded each measurement automatically. The digital controller of the data logger was linked to the testing machine. After each loading step, the magnitude of the applied load, deflection at the mid-span, crack width, and strain in both the steel reinforcement bars and the concrete surface were measured and recorded.

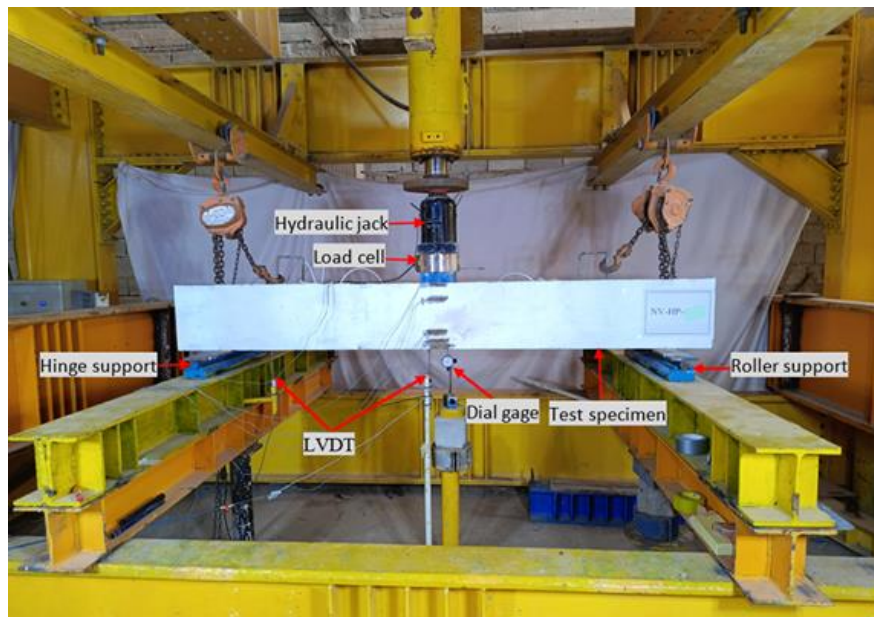


Figure 5. Experimental test setup

3. Experimental Outcomes and Discussion

3.1. Mechanical Properties of Concrete Mixes

Figures 6 to 9 display the concrete mix mechanical properties tests, and Table 7 illustrates the mechanical properties of the two considered concrete mixes (plain & fibrous type) used for different specimens investigated in this study. From the results, it can be observed that the inclusion of 1% hooked-end steel fiber and 0.5% macro polypropylene fiber led to a relatively small increase in the compressive strength of SCC. Where the compressive strength of cubes had increased by 17.11% at 28 days and by 12.75% at test time, while the compressive strength of concrete cylinders had increased by 9.73% at the test time. The tensile strength of SCC increased by 48 % when the hybrid fibers were included, and the modulus of rupture was enhanced by 26% when the hybrid fibers were added.



Figure 6. Cube compressive strength test (a) during test (b&c) after test (b) control mix (c) fiber mix



Figure 7. Compressive strength test (a) during test (b&c) after test (b) control mix (c) fiber mix

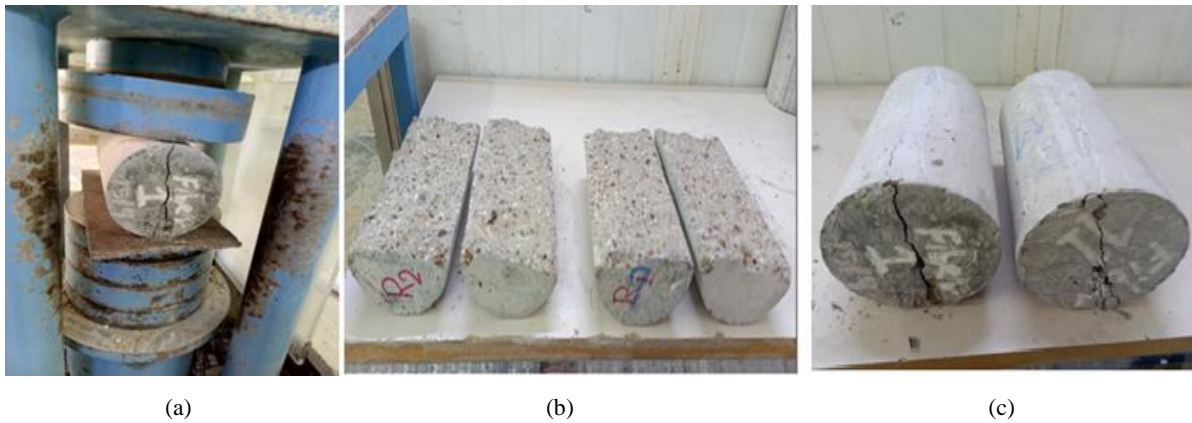


Figure 8. Splitting strength test (a) during test (b&c) after test (b) control mix (c) fiber mix

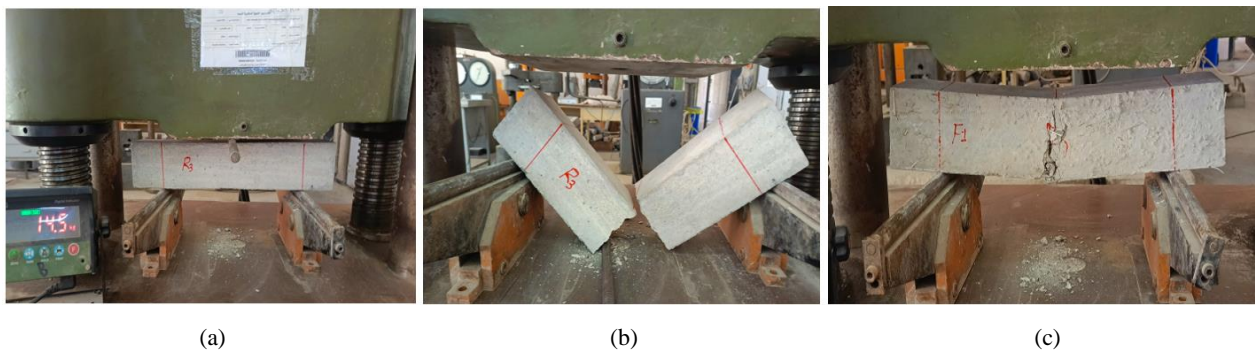


Figure 9. Modulus of rupture test (a) during the test (b&c) after the test (b) control mix (c) fiber mix

Table 7. Hardened concrete mechanical properties

Mix type	At 28 days		At test time		$\frac{f_c}{f_{cu}}$	At 28 days		At test time		Predicted f_t by ACI 318-19	f_r MPa	E_c MPa	Predicted E_c by ACI 318-19
	f_{cu} MPa	f_c MPa	f_{cu} MPa			f_t MPa	f_t MPa						
Plain mix	52.75	45.93	58.13	0.79	3.285	3.856	3.795	4.96	31480	31853			
Fibrous mix	61.78	50.4	65.54	0.77	4.877	5.708	3.976	6.248	39148	33367			

3.2. Load-Deflection Behavior, Crack Propagation, and Failure Mode

Figures 10 and 11 summarize the flexural load against mid-span deflections of all tested specimens. The yielding point was specified according to the methodology described by Park [36], and the serviceability limit was considered to be (60%) of the ultimate flexural load. The failure load and associated failure deflection are considered at longitudinal reinforcement fracture or concrete crushing, and the outcomes of the flexural behavior of all tested specimens are tabulated in Table 8.

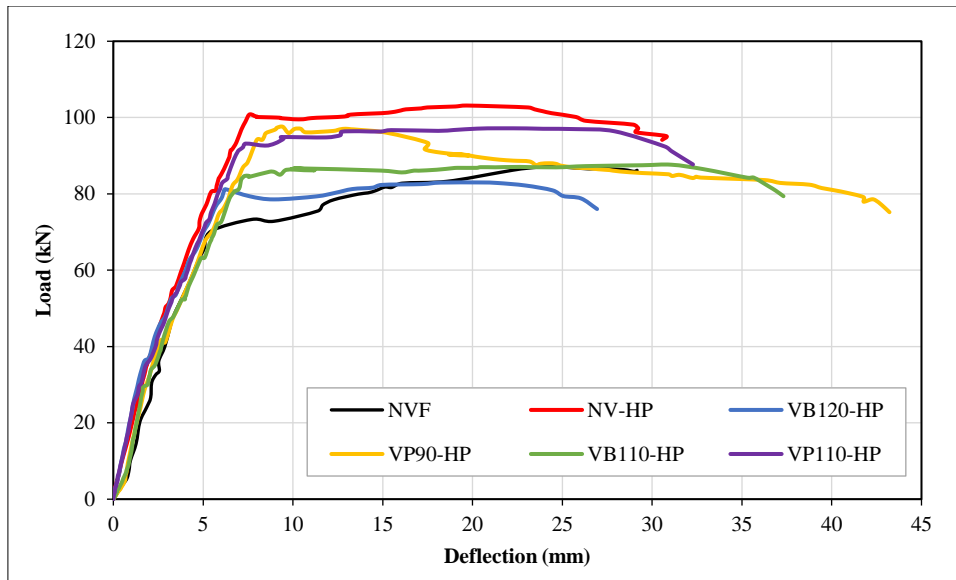


Figure 10. Comparison in load-vertical deflection curve at the midspan section of the tested specimens

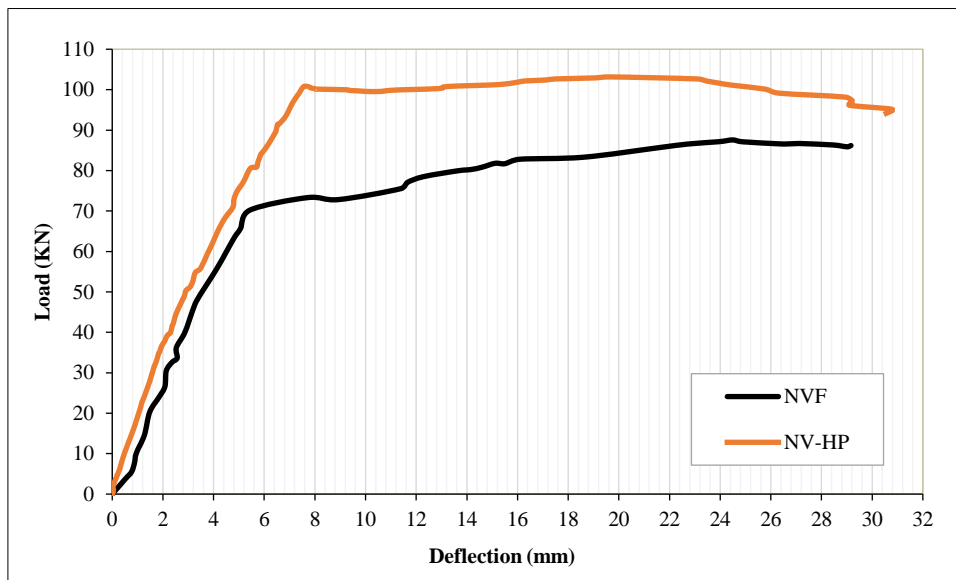


Figure 11. Effect of hybrid fiber on solid SCC beam flexural behavior

Table 8. Experimental results of tested beams

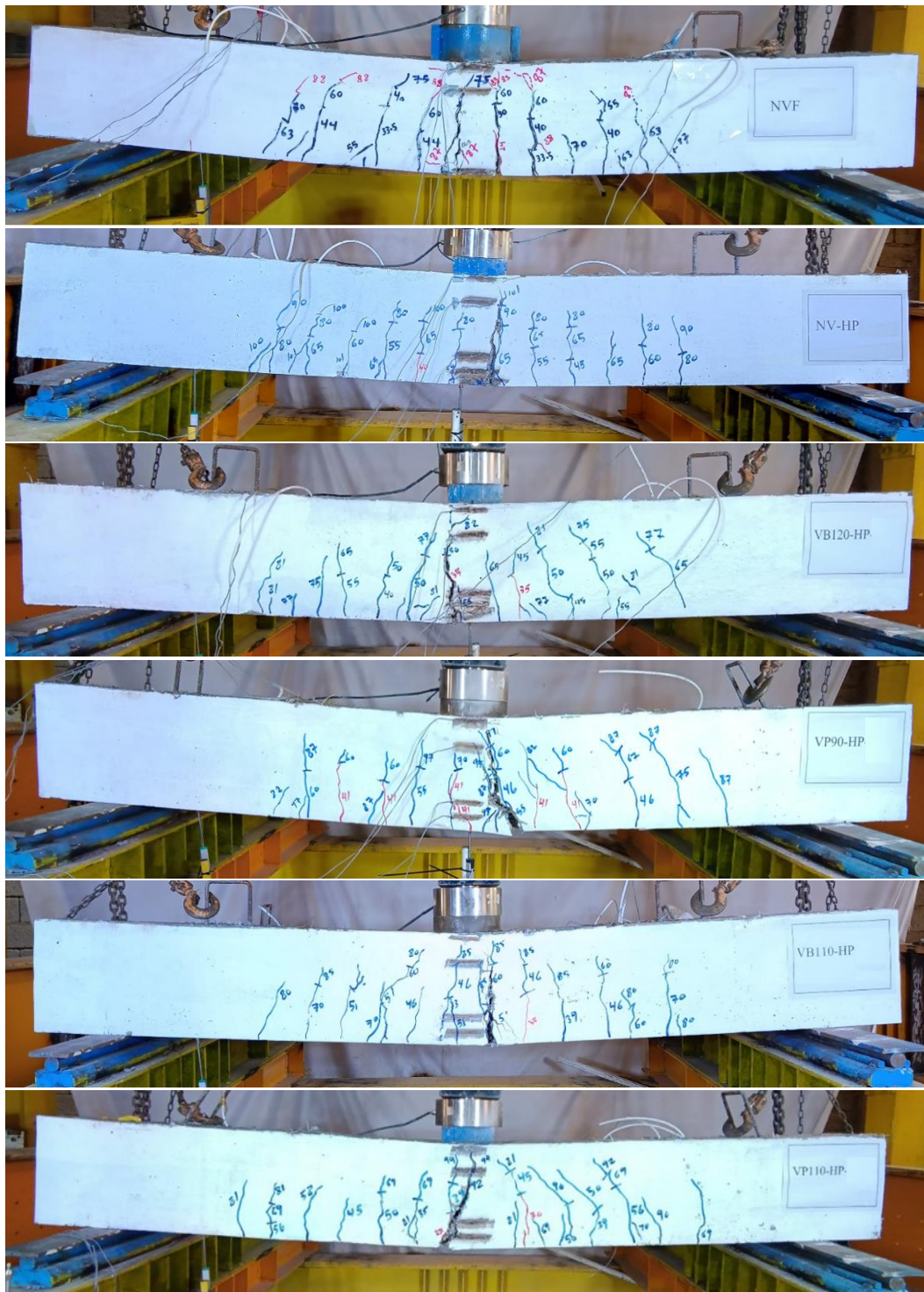
Beam Specimen	Initial-crack stage		Service stage		Yielding stage		Ultimate stage		Failure stage
	P_{CR} (kN)	Δ_{CR} (mm)	$P_{service}$ (kN)	$\Delta_{service}$ (mm)	P_y (kN)	Δ_y (mm)	P_u (kN)	Δ_u (mm)	Δ_f (mm)
NVF	24	1.85	56.6	4.23	70.0	5.35	88.0	23.33	29.16
NV-HP	40	2.27	67.00	4.40	96.0	7.00	103.0	19.67	30.56
VB120-HP	30	1.902	54.00	3.52	76.0	5.62	84.0	20.40	26.94
VP90-HP	28	1.72	63.00	4.75	88.0	7.35	97.0	9.43	43.22
VB110-HP	35	2.15	56.70	4.25	83.0	7.12	87.2	29.44	37.32
VP110-HP	27	1.807	63.20	4.37	91.2	6.9	97.18	21.50	32.28

3.2.1. Impact of Hybrid Fiber

Figure 11 illustrates the relation between flexural load and mid-span deflections of two solid beams, NVF (without fibers) & NV-HP (with fibers). It was detected that the incorporation of hybrid fibers enhanced the ultimate flexural load and the post-cracking flexural stiffness of the SCC beam. Because the cracks were prevented from propagating to the compressive zone, the fibrous beam showed significantly more flexural stiffness than the non-fibrous beam after the first cracking stage. By including macro polypropylene fiber and hooked-end steel fiber, the lower surface of RC beams could successfully prevent the formation of flexural cracks; this increased the effective cross-sectional area that resisted the bending moment in the fibrous beams, as found in the study of Banthia & Nandakumar [37].

The cracking, serviceability, yielding, and peak load for non-fibrous beams were 24, 56.6, 70, and 88 kN, respectively, while for fibrous beams (NV-HP) were 40, 67, 96, and 103, respectively. The incorporation of hybrid fiber improved the cracking, serviceability, yielding, and peak load by 66.67%, 18.37%, 37.14%, and 18.4 %, respectively, compared to non-fibrous beams. The midspan deflections corresponding to the yielding point increased by 30.84%, but to the peak point, they were decreased by 15.7 % when including the fibers due to the enhancement of flexural stiffness. The first crack width for the fibrous beam (0.037 mm) was less than the non-fibrous beam (0.056 mm).

The final state of crack patterns for the six full-scale self-consolidating beams is presented in Figure 12. Based on the test findings, the two solid beams failed in a flexure mode. The following can be used to characterize the overall response of these specimens: at the first stage of the test under a relatively low load level, the initial tension crack appeared close to the mid-span zone (maximum bending moment zone) because the concrete was weak in tension, which was indicative of the cracking load, and then multiple small flexural cracks appeared. With an increase in load, the cracks grew wider and expanded upward, and further, more cracks appeared in this area. Most of the cracks were developed before the longitudinal reinforcing bars began yielding. After that, at least one crack started to open unsteadily and propagated upward.



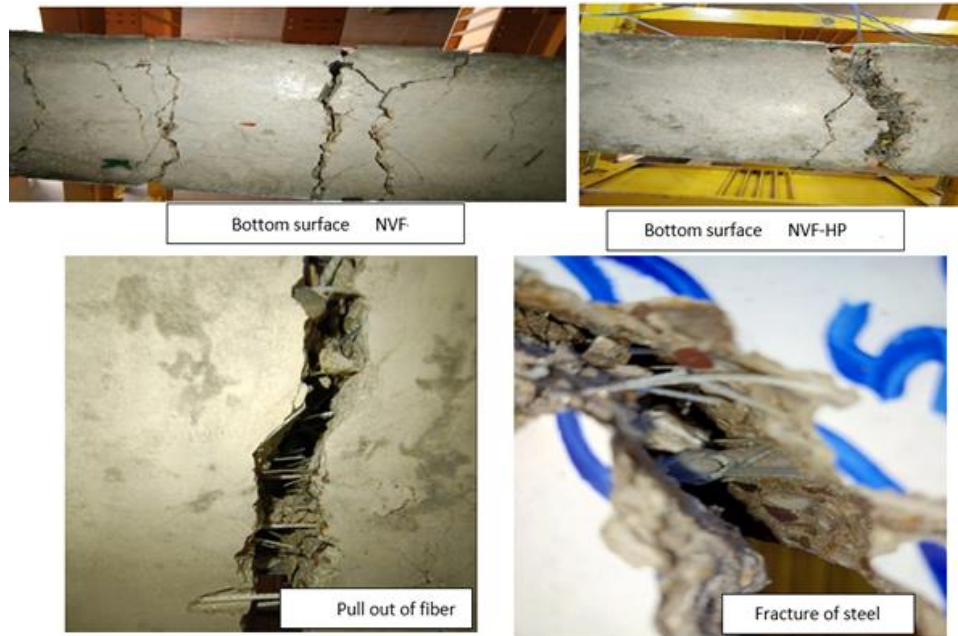


Figure 12. Crack patterns and failure mechanism of the tested specimens

For specimen NVF, the load-following crack localization progressively increased as the strain hardening of the longitudinal reinforcement steel. Complete failure was initiated by fracture of the longitudinal steel bars followed by crushing of the plain concrete matrix. At the peak load, the three major cracks extended up the compression zone. The initial crack appeared at 24 KN with a width of 0.056 mm, then other tiny flexural cracks also appeared in the maximum moment region of the beam. As the external load increased, evenly spaced flexural cracks continued to develop. Three major flexural cracks (10-18 mm wide) were observed in the maximum moment region and 11 additional hairline-thick flexural cracks distributed along the beam length.

For specimen NV-HP, after the localization of cracks and quick strain hardening of the steel bar reinforcement, load capacity slightly increased. The beams subsequently failed to carry loads because of the loss of fiber-bridging ability, leading to fracture of reinforcing steel. The failure happened because a large crack expanded noticeably to the compressive region after the steel bar yielded. As a result, the enormous energy stored in the hybrid fiber was released when the fiber was pulled out of the concrete mix, which caused the breaking of the steel bar and the beam failing as a result. The width of the major crack was larger than that of the other cracks. The final crack pattern of NV-HP is represented by one major crack of width 20 mm and 16 hairline-thick flexural cracks distributed along the flexural zone length of the beam. This phenomenon of cracking was found in previous literature [38-42].

The compression concrete zone under the applied load of the reference beam reached a strain of 0.001355 at the peak load stage and 0.00305 at the failure stage, while the strain of the extreme compression fiber of the fibrous beam (NV-HP) was 0.00113 & 0.00194 at the peak and failure stages. NVF exhibited significant spalling and crushing, while the NV-HP beam preserved the integrity of the concrete cover due to fiber-bridging, which stopped rapid compression force loss and severe spalling, and also the tension reinforcement at the bottom of the beam continued hardening and supplied more load capacity, as shown in Figure 13.

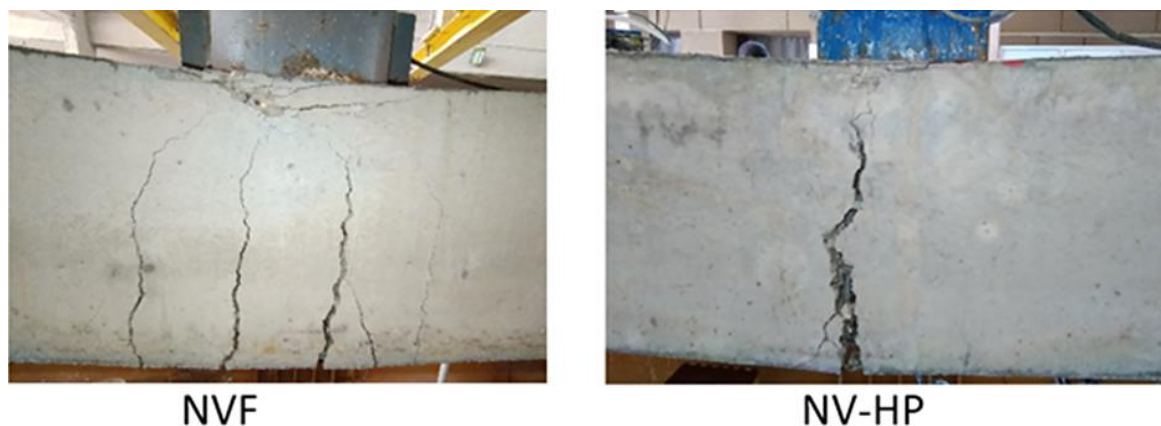


Figure 13. Compressive zone behavior after longitudinal steel fracture

3.2.2. Effect of Voids Shape and Size

From Figure 12, it is evident that the failure mode of the voided fibrous beams was similar to that of the solid beam (NV-HP), indicating that the presence of voids had an insignificant impact on the failure mechanism of fibrous beams. The failure of the voided fibrous beams was primarily caused by fiber pullout at a major flexural crack. These cracks propagated in the zone of maximum stress, resulting in a single dominant crack with a wider opening compared to the others, ultimately leading to the rupture of the steel bars. This rupture was typically preceded by minor crushing at the upper surface of the beam. Based on the observed crack patterns, the voided beams failed predominantly in flexural mode. The number of cracks ranged between 17 to 21, distributed along the beam's length. In the voided beams (VP90-HP and VP110-HP), cracks were observed to incline diagonally towards the regions of applied load.

The slope of the elastic portions of the load-deflection curves remained nearly constant across all beams, despite variations in the cracking loads, as shown in Figure 8. The influence of void dimensions became more pronounced after the onset of cracking. Initially, the effect of the longitudinal circular voids and bubbles was minimal, but as cracks began to develop and propagate towards the void boundaries, their impact became significant. This behavior can be attributed to the relative positioning of the longitudinal voids away from the zones of high initial stresses at the beam's lower surface prior to cracking. However, as the loading increased, the stress at the bottom levels near the voids also rose, leading to variations in cracking loads depending on the size of the voids. Cracks in the voided beams appeared earlier compared to the solid beams. The results for the first cracking load demonstrated that the presence of voids reduced the beam's resistance. Nevertheless, all voided beams exhibited a higher first cracking load compared to the non-fibrous beam (NVF).

For bubble beams, when the void diameter increased from 110 mm to 120 mm (R increasing from 8.13% to 9.8%), the first cracking load decreased by 14.3%. In the case of the bubble-voided beam (VB120-HP) and the longitudinal circular voided beam (VP90-HP), which had nearly the same concrete reduction volume (9.8%), the cracking loads were almost identical (30 kN and 28 kN, respectively). Compared to the solid fibrous beam (NV-HP), the cracking load decreased by 25% and 30%, respectively. For continuous longitudinal circular voided beams, when the void diameter increased from 90 mm to 110 mm (R increasing from 9.8% to 14.73%), the first cracking load decreased by 3.6%.

For beams with the same void diameter (110 mm) in both bubble and continuous longitudinal circular void configurations, the cracking load of VB110-HP was higher than that of VP110-HP by 22.86%. This was because the concrete reduction volume for the continuous circular voided beam (VP110-HP, 14.73%) was greater than that for the bubble-voided beam (VB110-HP, 8.13%). Compared with the solid fibrous beam (NV-HP), the cracking load decreased by 12.5% and 32% for VB110-HP and VP110-HP, respectively.

The same trend was observed for the yielding, serviceability, and ultimate loads. The yielding loads of all voided beams were higher than those of the non-fibrous beams, and the ultimate loads of voided beams were either higher than or equal to those of the non-fibrous beams, except for VB120-HP, which exhibited a slightly lower ultimate load by 4.6%. When compared to the solid fibrous beam (NV-HP), the loads at different stages for all voided beams decreased within the following ranges: 5.7%–19.4% at the serviceability stage, 5%–20.8% at the yielding stage, and 5.7%–18.5% at the ultimate stage.

The presence of voids in fibrous beams resulted in a decrease in load capacity, as they reduced the section moment of inertia, leading to a reduction in flexural rigidity and, consequently, a decrease in the ultimate load. Based on the results, it is evident that using PVC pipes to create longitudinal circular voids reduced the rate of load capacity decrease compared to bubble voids. This is attributed to the elasticity and high tensile strength of the PVC pipe. The ultimate loads for beams VP90-HP and VP110-HP decreased by approximately 5.83% and 5.6%, respectively, whereas for VB110-HP and VB120-HP, the reduction ratios were 15.34% and 18.45%, respectively.

When the bubble diameter increased from 110 mm to 120 mm (corresponding to an increase in R from 8.13% to 9.8%), the carrying loads decreased by 4.76%, 8.43%, and 3.93% at the serviceability, yielding, and ultimate load stages, respectively. For the bubble-voided beam (VB120-HP) and the longitudinal circular voided beam (VP90-HP), which had nearly the same concrete reduction volume (9.8%), the load capacities of VP90-HP were higher than those of VB120-HP by 16.7%, 15.8%, and 15.77% at the serviceability, yielding, and ultimate load stages, respectively. For beams with the same void diameter (110 mm) for both bubble and continuous longitudinal circular voids, the loads for VP110-HP were higher than those for VB110-HP by 10.46%, 9.9%, and 11.32% at the serviceability, yielding, and ultimate stages, respectively. Additionally, when the pipe diameter increased from 90 mm to 110 mm, the loads at the serviceability and ultimate stages remained almost the same; however, at the ultimate stage, VP110-HP exhibited a higher load than VB110-HP by 3.63%.

3.3. Ductility

Ductility is defined as the ability of a material to undergo significant plastic deformation beyond the elastic limit while maintaining a considerable load-bearing capacity up until complete failure. It is possible to measure ductility by

energy or deformation criteria. The deformation may appear as curvature, strain, or deflection. When using the deflection method, the most crucial factor to take into account when assessing ductility is the maximum deflection (Δ_f) that a material can withstand before failing. The deflection ductility index, μ_D , is represented as Δ_f / Δ_y , where Δ_f is the failure deflection (at the test end) and Δ_y is the deflection when steel reinforcement yielded. When using an energy-based method, ductility is characterized as the ability of inelastic energy absorption without compromising load capacity. The ductility index was calculated using Equation 1, which is derived from the energy area ratio theory suggested by Taerwe et al. [43] and it has been used in some previous studies [44-47], as shown in Figure 14.

$$\mu_E = \frac{1}{2} \left(\frac{E_{tot}}{E_{el}} + 1 \right) \tag{1}$$

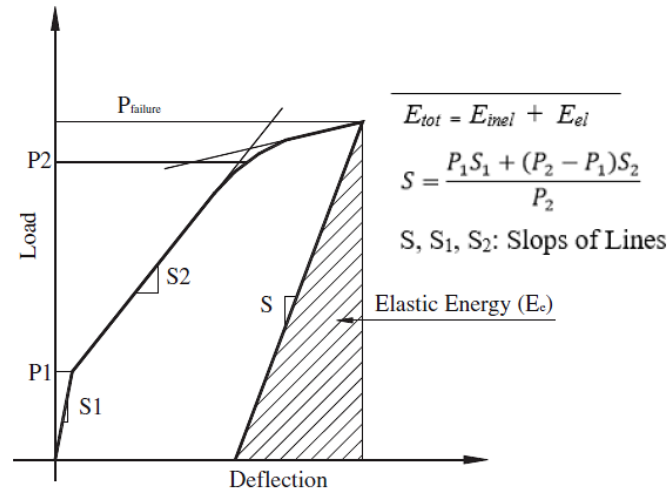


Figure 14. Definition for energy -ductility index by BS 1881-116 [32]

In this study these two methods were implemented based on load-displacement curves of tested specimens, and the results were tabulated in Table 9.

Table 9. Ductility indexes depended on deflection and energy-based methods

Specimen	S	E _{el} (kN.mm)	E _{tot} (kN.mm)	μ _E	μ _D
NVF	10.62	324	2123	3.780	5.45
NV-HP	12.82	352	2749	4.405	4.366
VB120-HP	12.29	235	1976	4.704	4.794
VP90-HP	11.26	245	3519	7.680	5.88
VB110-HP	11.13	279	2939	5.762	5.24
VP110-HP	12.43	305	2778	5.062	4.678

According to reports in the literature, structures constructed in high-seismic zones must achieve a ductility index of at least 3. As shown in Table 9, all the tested specimens demonstrated a ductility index greater than 3 based on both ductility evaluation methods. Using the deflection method, the solid fibrous beam (NV-HP) exhibited a ductility index that was 19.8% lower than that of the non-fibrous beam (NVF). Similar behavior has been reported in references [24, 48–50], which explained that this phenomenon is due to crack localization. In fiber-reinforced concrete, at the ultimate stage, when fibers are pulled out, inelastic deformation becomes concentrated at one or two major cracks at the localization points. In contrast, non-fibrous beams develop several larger cracks, with the strain distributed along the length of the steel bars. Moreover, these studies also concluded that, for high-strength concrete (HSC) or ultra-high-performance fiber-reinforced concrete (UHPFRC) beams, the ductility index decreases as the reinforcement ratio increases. When steel fibers are added to beams, the deflection ductility (μ_D) tends to decrease because the steel fibers act as an additional reinforcement capable of carrying tensile stresses across crack surfaces, similarly to traditional steel reinforcing bars.

From the results based on the deflection method, it was observed that the deflection ductility of fibrous beams improved when voids were introduced. Specifically, the continuous circular voided beams (VP90-HP and VP110-HP) exhibited ductility indices 34.56% and 7.1% higher, respectively, compared to the solid fibrous beam (NV-HP). Similarly, the ductility enhancements for VB110-HP and VB120-HP were 19.9% and 9.7%, respectively, compared to NV-HP.

The effect of bubble size on the deflection ductility index was also examined: the beam VB110-HP exhibited a ductility index 8.5% higher than VB120-HP. Furthermore, the influence of void shape was investigated. For beams with pipe and bubble voids having nearly the same concrete reduction volume (VP90-HP and VB120-HP), the VP90-HP beam demonstrated a ductility index 22.6% higher than the bubble-voided beam (VB120-HP). However, for beams with the same void diameter (VB110-HP and VP110-HP), the bubble-voided beam (VB110-HP) exhibited a ductility index 10.73% higher than the pipe-voided beam (VP110-HP).

Based on the energy-based method, the results differed from those obtained using the deflection method, as illustrated in Figure 15. These differences arise because the ductility index of reinforced beams is influenced by various factors, such as fiber content, reinforcement ratio, and the tensile properties of the materials. The energy-based approach can effectively capture the advantages of incorporating hybrid fibers into concrete, particularly the improvement in ultimate bearing capacity and the corresponding deflection. The energy ductility (μ_E) increased by 16.54% with the addition of hybrid fibers, which is consistent with the findings of the previous study by Abbas et al. [7]. Moreover, among the fibrous beams, the VP90-HP specimen exhibited the highest μ_E value of 7.68, representing a 74% enhancement compared to the solid fibrous beam.

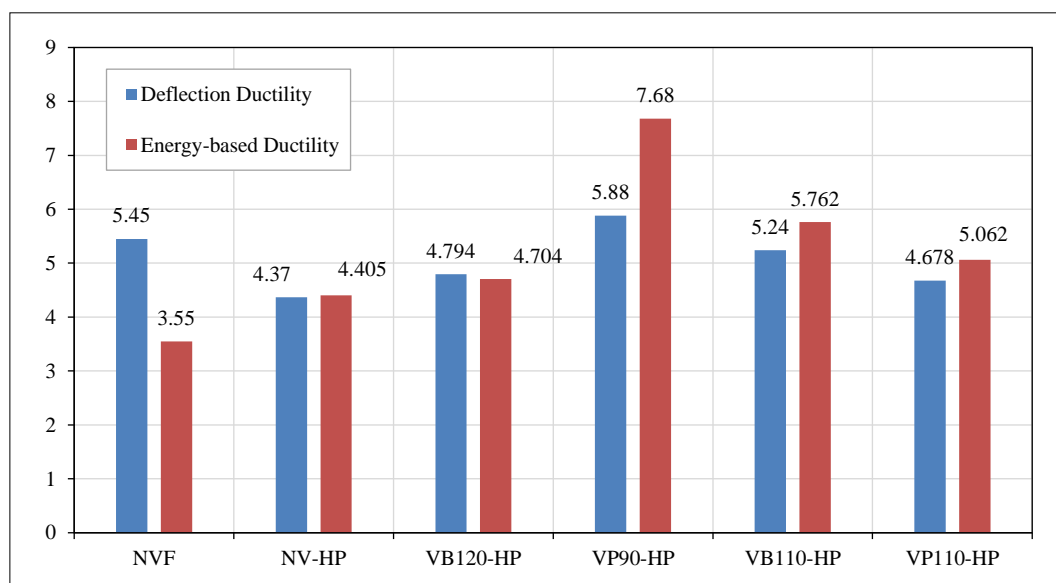


Figure 15. Ductility index for tested beams

3.4. Flexural Toughness and Stiffness

The flexural toughness of self-compacted hybrid fiber-reinforced concrete can be estimated using several methods, as outlined by Aslani and Samali [51] and in the ACI 544.4R-88 Report [52]. In this study, the flexural toughness of the specimens was evaluated by calculating the area under the load-deflection curve during flexural testing. Flexural toughness is defined as the total amount of energy absorbed by a specimen prior to failure.

The results of the calculated absorbed energy are presented in Table 10. The absorbed energy was assessed at three stages of the loading process: the first stage corresponds to the energy absorbed up to the first cracking, the second stage up to the serviceability limit, and the third stage represents the total energy absorbed until failure.

Table 10. Stiffness and Absorb energy for the tested beams

Beam Specimen	Stiffness K (kN/mm)	Absorb Energy (kN.mm)				
		E_{cr}	$E_{service}$	E_{ul}	$E_{cr}/E_{ul}\%$	$E_{service}/E_{ul}\%$
NVF	12.90	19.53	118.8	2123	0.92	5.6
NV-HP	17.84	50.34	168.5	2749	1.83	6.13
VB120-HP	15.60	28.12	112	1976	1.42	5.67
VP90-HP	16.30	20.61	166.8	3519	0.59	4.74
VB110-HP	16.66	41.15	132	2936	1.402	4.5
VP110-HP	14.97	18.77	165.9	2778	0.676	6.0

The influence of hybrid fibers on the overall toughness can be observed from the results of beams NVF and NV-HP. It is evident that the addition of hybrid fibers (1% hooked steel fibers and 0.5% macro polypropylene fibers) increased the toughness by 157.8%, 41.84%, and 29.55% at the cracking, serviceability, and ultimate stages, respectively. This improvement is attributed to the enhanced load absorption during the cracking and yielding phases due to the fiber-bridging mechanism.

In fibrous beams, the inclusion of air voids led to a reduction in toughness at the cracking and serviceability stages by 18.3% to 62.7% compared to the solid fibrous beam (NV-HP), because these beams absorbed lower loads and exhibited lower or only slightly higher deflections than the solid fibrous beam at these stages — and toughness depends on both load and deflection. At the ultimate stage, however, the voided beams exhibited higher toughness values than the solid beam NV-HP (except for VB120-HP), with increases ranging from 1.1% to 28%. This is mainly explained by the larger retained deformations prior to failure.

When the bubble diameter increased from 110 mm to 120 mm (corresponding to a rise in R from 8.13% to 9.8%), the total toughness decreased by 32.7%. Similarly, when the pipe diameter increased from 90 mm to 110 mm, the toughness decreased by 21%. For beams with different void shapes (bubble and pipe) but with the same concrete reduction volume (R = 9.8%), the toughness of VP90-HP was 78% higher than that of VB120-HP. However, for beams with different void shapes but the same diameter of 110 mm, the total toughness of VB110-HP was 5.7% higher than that of VP110-HP.

Stiffness was determined based on the elastic portion of the load-deflection curves. The elastic stiffness of the solid beam improved with the addition of hybrid fibers, with the stiffness of NV-HP increasing by 38.3% compared to the non-fibrous beam (NVF). In fibrous beams, the inclusion of voids led to a decrease in stiffness by 6.61% to 16.09%. It was also observed that the stiffness of fibrous specimens (both solid and voided) was greater than that of the non-fibrous specimen (NVF). As the diameter of the pipe and bubble voids increased, stiffness decreased — for instance, the stiffness of VP110-HP was 8.2% lower than that of VP90-HP, and the stiffness of VB120-HP was 6.36% lower than that of VB110-HP.

3.5. Load- Strain Relationships

The strains in the concrete surface, longitudinal steel bars, and stirrups were measured using electrical-resistance strain gauges installed at several selected locations, as shown in Figure 16. The strains were continuously and automatically monitored throughout the entire testing process. The strain data recorded from gauges installed on the steel reinforcement bars at mid-span (SG-5 and SG-6) of all tested specimens are presented in Figure 17. The load–steel strain relationships for the plain and fibrous SCC solid beams at various load levels are illustrated in Figure 18. The graph shows that the addition of hybrid fibers has a minor effect on the steel reinforcement strains before cracking occurs in the SCC beam. Up to the cracking load of the control beam (NVF) at 24 kN, the steel reinforcement strains of both NVF and NV-HP beams were almost identical. However, after cracking developed in the fibrous SCC beam, the strain experienced by the longitudinal reinforcement was significantly reduced due to the presence of hybrid fibers, compared to the control beam. For instance, at a load level of 60 kN, the steel reinforcement strain was reduced by 45.3% with the addition of hybrid fibers.

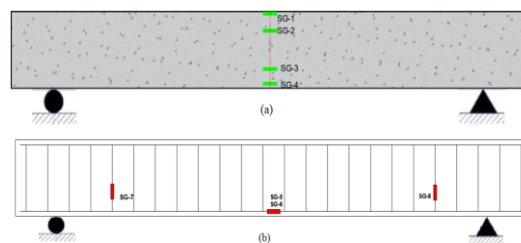


Figure 16. Location of strain gauges (a) at concrete side surface (b) at steel

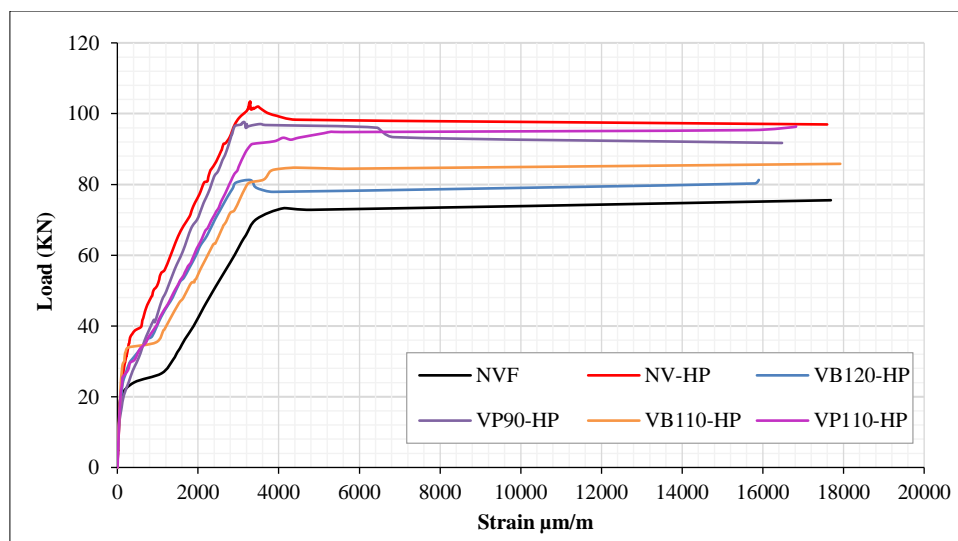


Figure 17. Load-longitudinal steel bar strain curves (SG-5)

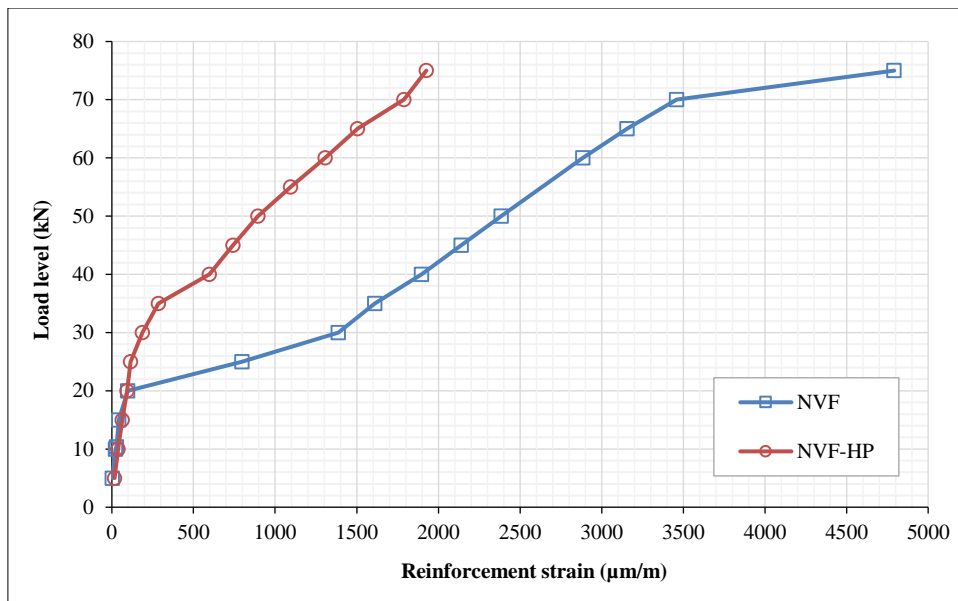


Figure 18. Effect of hybrid fibers on steel bar strain (SG-5) at different load levels for solid beams

Before the appearance of cracks, there was strain compatibility among the concrete, steel reinforcement, and hybrid fibers. At this stage, the role of hybrid fibers in enhancing the concrete's tensile strength was limited. After cracking, this strain compatibility was disrupted, and the hybrid fibers bridged across the cracks to transfer loads alongside the traditional steel reinforcing bars, significantly reducing the strain experienced by the steel reinforcement compared to beams without fibers under equivalent loading conditions.

Figure 19 illustrates the strain distribution in the concrete and steel bars at corresponding locations (SG4 and SG5) in the VP110-HP beam. It can be observed that strain compatibility between the steel reinforcement bars and the surrounding concrete was maintained up to the cracking load (27 kN). After cracking, the strain in the concrete exceeded that in the steel bars, due to the presence of fibers that bridged the cracks and helped sustain the load together with the longitudinal reinforcement, thereby reducing the strain carried by the steel bars.

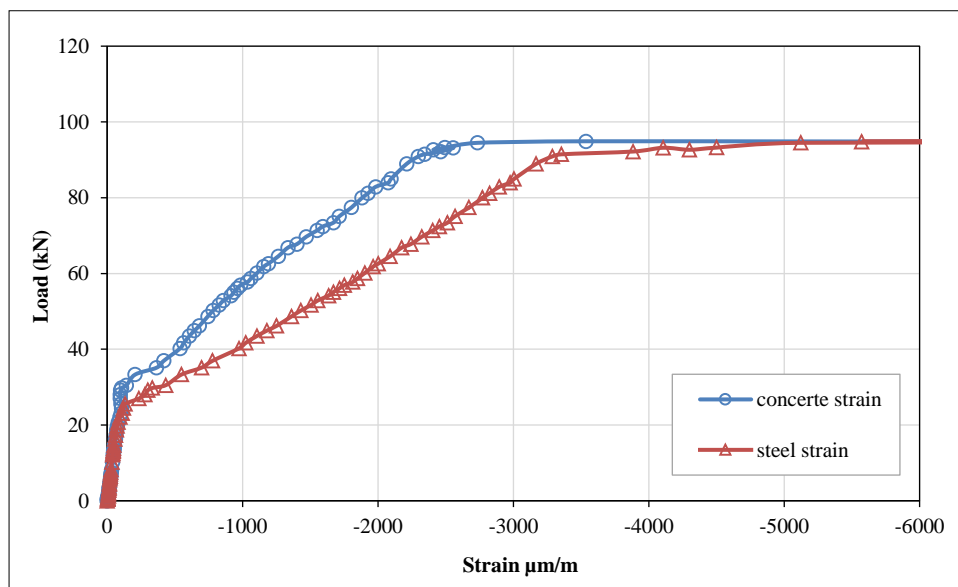


Figure 19. Load -Strain curve for (SG4 &SG5) of a beam VP110-HP

Voided beams exhibited lower steel strain values at the first cracking stage compared to the solid fibrous beam (NV-HP), but showed higher steel strains at the ultimate stage. At the cracking stage, the steel strain was reduced by 29.6% to 66.4%, depending on the size and shape of the voids. As shown in Table 11, at the ultimate stage, the steel strain in the non-fibrous beam (NVF) reached 17,686 µε, which is close to the rupture strain. This occurred because the steel bars alone resisted the tensile stresses that developed after cracking. A similar behavior was observed in the voided beams VP110-HP and VB110-HP, where the reduction in sectional area combined with a diminished fiber-bridging effect at the crack interfaces led to comparable steel strain values.

Table 11. Variation of longitudinal steel bar stain at mid-span at different loading stages

Specimen	ϵ_{cr}	$\epsilon_{service}$	ϵ_y	ϵ_u
NVF	413	2675	3410	17686
NV-HP	554	1565	2860	3555
VB120-HP	186	1647	2760	3298
VP90-HP	390	1682	2660	3150
VB110-HP	242	1800	3050	17919
VP110-HP	322	2018	3855	16823

Based on Table 12 and Figure 20, the findings indicated that as the load increased, the strain in the extreme compression fiber at mid-span also increased. Compared to the non-fibrous beam (NVF), the strains at the extreme compression fiber of the solid fibrous specimen (NV-HP) were higher during both the first cracking and yielding phases. These results support the conclusion previously discussed, namely that the flexural capacity of the SCC hybrid fiber beam was greater during the cracking and yielding stages. This enhancement is attributed to the presence of hybrid fibers in the SCC, which helped prevent crack widening and delayed the progression of cracking and yielding, thereby increasing the strain in the compression fiber of the specimens.

Table 12. Variation of stain at the compression fiber (SG-1) at different loading stages

Specimen	ϵ_{cr}	$\epsilon_{service}$	ϵ_y	ϵ_u	ϵ_{max}
NVF	166	546	670	1323	3050
NV-HP	297	595	935	1113	1940
VB120-HP	209	500	730	1410	1890
VP90-HP	190	620	912	1195	2605
VB110-HP	240	472	745	1611	1920
VP110-HP	162	524	840	2050	2050

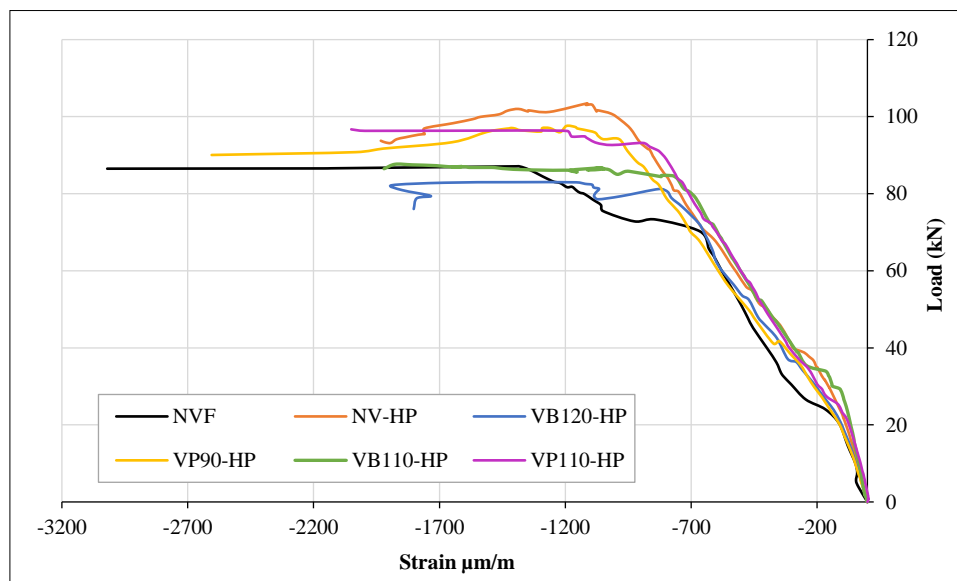


Figure 20. Load-concrete strain curves for tested beams

Additionally, during the failure stage, the upper fiber of the non-fibrous beam (NVF) experienced a strain of 3048 microstrain, whereas the upper fiber of the fibrous beam (NV-HP) experienced a strain of 1940 microstrain. This indicates that the NVF beam exhibited significant spalling and crushing, while the NV-HP beam maintained the integrity of the concrete cover. This behavior is attributed to the fiber-bridging effect, which prevents rapid loss of compressive forces and severe spalling, as shown in Figure 13.

In fibrous beams, when voids were introduced, the concrete strain (measured by SG-1) decreased at the cracking and yielding stages, but increased at the ultimate stage. The strain in fibrous beams decreased by 9.2% to 59.5% at the cracking load and by 2.5% to 22% at the yielding stage. However, at the ultimate stage, the strain increased by 7.4% to 84%, depending on the size and shape of the voids.

4. Conclusions

The flexural behavior of self-compacted solid and voided reinforced concrete (RC) beams incorporating hybrid fibers (1.0% hooked steel fibers and 0.5% macro polypropylene fibers) was evaluated experimentally. Tests were conducted on six self-compacted RC beams under three-point static loading in a simply supported setup. The following key findings were drawn:

- The use of 1.0% hooked steel fibers and 0.5% macro polypropylene fibers successfully maintained the workability of the self-compacted concrete mix.
- Incorporating 1% hooked steel fibers and 0.5% macro polypropylene fibers into the self-consolidating concrete mix enhanced the mechanical properties of the concrete, with increases in tensile strength, compressive strength, and modulus of rupture by 48%, 9.73%, and 26%, respectively.
- The flexural strength at the cracking, serviceability, yielding, and peak load stages of self-compacted beams significantly improved with the addition of hybrid fibers to the solid beam, while the midspan deflection associated with peak load decreased. The first crack width in the fibrous beam (0.037 mm) was smaller than that in the non-fibrous beam (0.056 mm).
- When voids were incorporated into the fibrous beams, the loads at various stages decreased. This reduction was attributed to a lower moment of inertia, leading to decreased flexural rigidity and, consequently, a reduced ultimate load.
- All tested beams (plain solid, fibrous solid, and fibrous voided) failed in flexural mode.
- When hybrid fibers were incorporated into the concrete mix of both solid and voided beams, failure occurred due to a major crack expanding into the compression region after yielding of the steel bars. Upon fiber pullout, the significant energy stored in the fibers was released, leading to steel bar fracture and beam failure — a mechanism referred to as crack localization.
- The presence of voids had no significant impact on the failure mechanism of fibrous beams; failure in voided fibrous beams was caused by fiber pullout at a major flexural crack, similar to the solid fibrous beams.
- Based on the ultimate deflection method, the ductility index decreased by 19.8% with the addition of hybrid fibers, due to reduced deflection resulting from improved flexural stiffness. However, the ductility index based on the energy method improved by 16.54% with the inclusion of hybrid fibers, effectively capturing the benefits such as increased ultimate load capacity and associated deflection.
- The ductility of fibrous beams can be enhanced when the air voids are included in them depending on two methods. Among the voided fibrous beams, the VP90-HP specimen exhibited the highest μ_D & μ_E values of 5.88 & 7.68 with enhancement ratios of 34.56 % & 74 % compared with fibrous solid beam.
- The ductility of fibrous beams could be enhanced by the inclusion of air voids, as demonstrated by two evaluation methods. Among the voided fibrous beams, specimen VP90-HP exhibited the highest μ_D and μ_E values of 5.88 and 7.68, with enhancement ratios of 34.56% and 74%, respectively, compared to the solid fibrous beam.
- The addition of hybrid fibers increased the energy absorption capacity of the beams at the cracking, serviceability, and ultimate stages due to the fiber-bridging action.
- In fibrous beams, the inclusion of air voids with a concrete volume reduction of 8%–14.73% resulted in toughness values at the cracking and serviceability stages that were 18.3% to 62.7% lower than those of the solid fibrous beams; however, at the ultimate stage, voided beams exhibited higher toughness than the solid beams.
- The elastic stiffness of the solid beam increased by 38.3% with the addition of hybrid fibers. In fibrous beams, the inclusion of voids led to a decrease in stiffness by 6.61% to 16.09%. Nevertheless, the stiffness of all fibrous beams (both solid and voided) remained higher than that of the non-fibrous beams.
- As the diameters of the pipe and bubble voids increased, the stiffness of the fibrous beams decreased.
- The inclusion of hybrid fibers had an insignificant impact on the strain in reinforcing steel bars before cracking, but contributed significantly to reducing steel bar strain in the post-cracking stage.
- Voided beams exhibited lower steel strain values at first cracking compared to the solid fibrous beam, but showed higher values at the ultimate stage. Steel strain reductions at the cracking stage ranged from 29.6% to 66.4%, depending on void size and shape.
- In fibrous beams with voids, the concrete strain at the extreme compression fiber decreased at the cracking and yielding stages, but increased at the ultimate stage, influenced by the size and shape of the voids.

5. Declarations

5.1. Author Contributions

Conceptualization, E.M.E. and S.D.M.; methodology, E.M.E. and S.D.M.; investigation, E.M.E. and S.D.M.; resources, E.M.E. and S.D.M.; data curation, E.M.E.; writing—original draft preparation, E.M.E.; writing—review and editing, E.M.E. and S.D.M.; visualization, E.M.E.; supervision, S.D.M.; project administration, E.M.E.; funding acquisition, E.M.E. All authors have read and agreed to the published version of the manuscript.

5.2. Data Availability Statement

The data presented in this study are available on request from the corresponding author.

5.3. Funding

The authors received no financial support for the research, authorship, and/or publication of this article.

5.4. Conflicts of Interest

The authors declare no conflict of interest.

6. References

- [1] Mansur, M. A. (1998). Effect of openings on the behaviour and strength of R/C beams in shear. *Cement and Concrete Composites*, 20(6), 477–486. doi:10.1016/S0958-9465(98)00030-4.
- [2] Mansur, M. A. (1999). Design of reinforced concrete beams with small openings under combined loading. *ACI Structural Journal*, 96(5), 675–682. doi:10.14359/720.
- [3] Nasvik, J. (2011). On the bubble: Placing concrete around plastic voids increases efficiency and reduces costs. *Concrete Construction - World of Concrete*, 56(12), 20–22.
- [4] Churakov, A. (2014). Biaxial hollow slab with innovative types of voids. *Construction of Unique Buildings and Structures*, (6), 70. (In Russian).
- [5] Mahdi, A. S., & Mohammed, S. D. (2021). Experimental and Numerical Analysis of Bubbles Distribution Influence in BubbleDeck Slab under Harmonic Load Effect. *Engineering, Technology & Applied Science Research*, 11(1), 6645–6649. doi:10.48084/etasr.3963.
- [6] Idris, N. A., Noh, H. M., Azwani Mohamad, N. L. I., & Bangau, R. (2020). Reinforced Concrete by Using the Rectangular Shape of Voided Beam. *Journal of Mechanical Engineering*, 9.
- [7] Abbass, A. A., Abid, S. R., Arna'ot, F. H., Al-Ameri, R. A., & Özakça, M. (2020). Flexural response of hollow high strength concrete beams considering different size reductions. *Structures*, 23, 69–86. doi:10.1016/j.istruc.2019.10.001.
- [8] Alnuaimi, A. S., Al-Jabri, K. S., & Hago, A. (2008). Comparison between solid and hollow reinforced concrete beams. *Materials and Structures/Materiaux et Constructions*, 41(2), 269–286. doi:10.1617/s11527-007-9237-x.
- [9] Dinesh Kanna, M., & Arun, M. (2021). Effects of Longitudinal and Transverse Direction Opening in Reinforced Concrete Beam: The State of Review. *IOP Conference Series: Materials Science and Engineering*, 1059(1), 12049. doi:10.1088/1757-899X/1059/1/012049.
- [10] Murugesan, A., & Narayanan, A. (2017). Influence of a Longitudinal Circular Hole on Flexural Strength of Reinforced Concrete Beams. *Practice Periodical on Structural Design and Construction*, 22(2), 04016021. doi:10.1061/(asce)sc.1943-5576.0000307.
- [11] Ismael, M. A., & Hameed, Y. M. (2022). Structural behavior of hollow-core reinforced self-compacting concrete beams. *SN Applied Sciences*, 4(5), 150. doi:10.1007/s42452-022-05036-6.
- [12] Al-Smadi, Y. M., Al-Huthaifi, N., & Alkhalwaldeh, A. A. (2022). The effect of longitudinal hole shape and size on the flexural behavior of RC beams. *Results in Engineering*, 16, 100607. doi:10.1016/j.rineng.2022.100607.
- [13] Sivaneshan, P., & Harishankar, S. (2017). Experimental Study on Voided Reinforced Concrete Beams with Polythene Balls. *IOP Conference Series: Earth and Environmental Science*, 80(1), 12031. doi:10.1088/1755-1315/80/1/012031.
- [14] Ajeel, A. E., Qaseem, T. A., & Rasheed, S. R. (2018). Structural behavior of voided reinforced concrete beams under combined moments. *Civil and Environmental Research*, 10(1), 17-24.
- [15] Hekal, G. M., Fadel, A. K., Shaheen, Y. B., & Fayed, S. (2025). Flexure strength of multi-hollow core RC beams reinforced with advanced materials. *Structures*, 71, 108051. doi:10.1016/j.istruc.2024.108051.
- [16] Olivito, R. S., & Zuccarello, F. A. (2010). An experimental study on the tensile strength of steel fiber reinforced concrete. *Composites Part B: Engineering*, 41(3), 246–255. doi:10.1016/j.compositesb.2009.12.003.

- [17] Soutsos, M. N., Le, T. T., & Lampropoulos, A. P. (2012). Flexural performance of fibre reinforced concrete made with steel and synthetic fibres. *Construction and Building Materials*, 36, 704–710. doi:10.1016/j.conbuildmat.2012.06.042.
- [18] Chi, Y., Xu, L., & Zhang, Y. (2014). Experimental Study on Hybrid Fiber-Reinforced Concrete Subjected to Uniaxial Compression. *Journal of Materials in Civil Engineering*, 26(2), 211–218. doi:10.1061/(asce)mt.1943-5533.0000764.
- [19] Adnan Hadi, M., & Mohammed, S. D. (2021). Improving torsional - Flexural resistance of concrete beams reinforced by hooked and straight steel fibers. *Materials Today: Proceedings*, 42, 3072–3082. doi:10.1016/j.matpr.2020.12.1046.
- [20] Ismael, T. M., & Mohammed, S. D. (2021). Enhancing the mechanical properties of lightweight concrete using mono and hybrid fibers. *IOP Conference Series: Materials Science and Engineering*, 1105(1), 012084. doi:10.1088/1757-899x/1105/1/012084.
- [21] Grünewald, S., & Walraven, J. C. (2001). Parameter-study on the influence of steel fibers and coarse aggregate content on the fresh properties of self-compacting concrete. *Cement and Concrete Research*, 31(12), 1793–1798. doi:10.1016/S0008-8846(01)00555-5.
- [22] Ayeni, I. S., Yatim, J. M., Shukor Lim, N. H. A., & Aluko, O. G. (2024). A Review of Hybridised Use of Fibres in Shear Behaviour of Fibre-Reinforced Concrete Beams. *ASEAN Engineering Journal*, 14(1), 145–156. doi:10.11113/aej.V14.20314.
- [23] Wu, F., Zhao, B., Cao, J., Shen, X., Wang, Z., Lei, H., & Cui, Z. (2024). Experimental and theoretical investigations on flexural performance of hybrid fiber reinforced ECC-NC composite beams. *Case Studies in Construction Materials*, 20, 3178. doi:10.1016/j.cscm.2024.e03178.
- [24] Yoo, D. Y., Soleimani-Dashtaki, S., Oh, T., Chun, B., Banthia, N., Lee, S. J., & Yoon, Y. S. (2024). Strain-hardening effect on the flexural behavior of ultra-high-performance fiber-reinforced concrete beams with steel rebars. *Developments in the Built Environment*, 17, 100343. doi:10.1016/j.dibe.2024.100343.
- [25] Sasikumar, P., & Candassamy, K. (2024). Strengthening of flexural behavior of reinforced concrete beams by using hybrid fibers: experimental and analytical study. *Revista de La Construcción*, 23(2), 354–373. doi:10.7764/RDLC.23.2.354.
- [26] Alshahrani, A., Kulasegaram, S., & Kundu, A. (2025). Utilisation of simulation-driven fibre orientation for effective modelling of flexural strength and toughness in self-compacting concrete. *Construction and Building Materials*, 459, 139767. doi:10.1016/j.conbuildmat.2024.139767.
- [27] Altun, F., Haktanir, T., & Ari, K. (2006). Experimental investigation of steel fiber reinforced concrete box beams under bending. *Materials and Structures/Materiaux et Constructions*, 39(4), 491–499. doi:10.1617/s11527-006-9095-y.
- [28] Jacob, B. M., & Bincy, S. (2018). Parametric Study of Longitudinal Hollow Steel Fibre Reinforced Concrete (SFRC) Beams. *IOP Conference Series: Materials Science and Engineering*, 396(1), 12011. doi:10.1088/1757-899X/396/1/012011.
- [29] EFCA. (2005). *The European Guidelines for Self-Compacting Concrete: Specification, Production and Use. The European Guidelines for Self-Compacting Concrete (Issue May)*. European Project Group. European Federation of Concrete Admixtures Associations (EFCA), Berlin, Germany.
- [30] ASTM C33/C33M-18. (2003). *Standard Specification for Concrete Aggregates*. ASTM International, Pennsylvania, United States. doi:10.1520/C0033_C0033M-18.
- [31] ASTM C39/C39M-18. (2020). *Standard Test Method for Compressive Strength of Cylindrical Concrete Specimens*. ASTM International, Pennsylvania, United States. doi:10.1520/C0039_C0039M-18.
- [32] BS 1881-116. (1983) *Testing Concrete. Method for Determination of Compressive Strength of Concrete Cubes*. British standard Institute (BSI), London, United Kingdom.
- [33] ASTM C496/C496M-17. (2017). *Standard Test Method for Splitting Tensile Strength of Cylindrical Concrete Specimens*, ASTM International, Pennsylvania, United States. doi:10.1520/C0496_C0496M-17.
- [34] ASTM C469/C469M-14. (2021). *Standard Test Method for Static Modulus of Elasticity and Poisson's Ratio of Concrete in Compression*, ASTM International, Pennsylvania, United States. doi:10.1520/C0469_C0469M-14.
- [35] ACI 318-19. (2019). *American Concrete Institute, Building Code Requirements for Structural Concrete*. American Concrete Institute (ACI), Farmington Hills, United States.
- [36] Park, R. (1988, August). Ductility evaluation from laboratory and analytical testing. *Proceedings of the 9th world conference on earthquake engineering*, 2-9 August, Tokyo-Kyoto Japan.
- [37] Banthia, N., & Nandakumar, N. (2003). Crack growth resistance of hybrid fiber reinforced cement composites. *Cement and Concrete Composites*, 25(1), 3–9. doi:10.1016/S0958-9465(01)00043-9.
- [38] Shao, Y. (2020). *Improving ductility and design methods of reinforced high-performance fiber-reinforced cementitious composite (HPFRCC) flexural members*. Ph.D. Thesis, Stanford University, Stanford, United States.

- [39] Dancygier, A. N., & Savir, Z. (2006). Flexural behavior of HSFRC with low reinforcement ratios. *Engineering Structures*, 28(11), 1503–1512. doi:10.1016/j.engstruct.2006.02.005.
- [40] Ning, X., Ding, Y., Zhang, F., & Zhang, Y. (2015). Experimental study and prediction model for flexural behavior of reinforced SCC beam containing steel fibers. *Construction and Building Materials*, 93, 644–653. doi:10.1016/j.conbuildmat.2015.06.024.
- [41] Chao, S. H., Naaman, A. E., & Parra-Montesinos, G. J. (2006). Bond behavior of strand embedded in fiber reinforced cementitious composites. *PCI Journal*, 51(6), 56–71. doi:10.15554/pcij.11012006.56.71.
- [42] Yoo, D. Y., & Yoon, Y. S. (2015). Structural performance of ultra-high-performance concrete beams with different steel fibers. *Engineering Structures*, 102, 409–423. doi:10.1016/j.engstruct.2015.08.029.
- [43] Taerwe, L. (2020). Structural ductility of concrete beams prestressed with FRP tendons. In *Non-Metallic (FRP) Reinforcement for Concrete Structures*. Non-Metallic (FRP) Reinforcement for Concrete Structures. doi:10.1201/9781482271621-56.
- [44] Li, Z., Zhu, H., Zhen, X., Wen, C., & Chen, G. (2021). Effects of steel fiber on the flexural behavior and ductility of concrete beams reinforced with BFRP rebars under repeated loading. *Composite Structures*, 270, 114072. doi:10.1016/j.compstruct.2021.114072.
- [45] Wang, H., & Belarbi, A. (2011). Ductility characteristics of fiber-reinforced-concrete beams reinforced with FRP rebars. *Construction and Building Materials*, 25(5), 2391–2401. doi:10.1016/j.conbuildmat.2010.11.040.
- [46] Natarajan, E. (2018). Ductility Response of Hybrid Fibre Reinforced Concrete Beams. *Journal of Urban and Environmental Engineering*, 174–179. doi:10.4090/juee.2017.v11n2.174-179.
- [47] Kim, T. K., & Park, J. S. (2021). Evaluation of the performance and ductility index of concrete structures using advanced composite material strengthening methods. *Polymers*, 13(23), 4239. doi:10.3390/polym13234239.
- [48] You, Z., Chen, X., & Dong, S. (2011). Ductility and strength of hybrid fiber reinforced self-consolidating concrete beam with low reinforcement ratios. *Systems Engineering Procedia*, 1, 28–34. doi:10.1016/j.sepro.2011.08.006.
- [49] Espion, B. (1994). Discussion of “Flexural Analysis of Reinforced Concrete Beams Containing Steel Fibers” by Byung Hwan Oh (October, 1992, Vol. 118, No. 10). *Journal of Structural Engineering*, 120(6), 1932–1934. doi:10.1061/(asce)0733-9445(1994)120:6(1932).
- [50] Ashour, S. A. (2000). Effect of compressive strength and tensile reinforcement ratio on flexural behavior of high-strength concrete beams. *Engineering Structures*, 22(5), 413–423. doi:10.1016/S0141-0296(98)00135-7.
- [51] Aslani, F., & Samali, B. (2014). Flexural toughness characteristics of self-compacting concrete incorporating steel and polypropylene fibres. *Australian Journal of Structural Engineering*, 15(3), 269–286. doi:10.7158/S13-011.2014.15.3.
- [52] ACI 544.4R-88 Report. (1999). Design Considerations for Steel Fiber Reinforced Concrete. *ACI Structural Journal*, 85(5), 544.4R-1-544.4R-17. doi:10.14359/3144.